Modern Applied Science; Vol. 8, No. 3; 2014
ISSN 1913-1844 E-ISSN 1913-1852
Published by Canadian Center of Science and Education

Annealing Effect of High Dielectric Material for Low Voltage Electrowetting on Dielectric (EWOD)

Hsiu-Hsiang Chen[1] & Chien-Chung Fu[2]

[1] Industrial Technology Research Institute, Taiwan

[2] Institute of NanoEngineering and Microsystems, National Tsing-Hua University, Taiwan

Correspondence: Hsiu-Hsiang Chen, Industrial Technology Research Institute, Taiwan. E-mail: susanchen@itri.org.tw

Received: February 10, 2014 Accepted: March 18, 2014 Online Published: April 8, 2014

doi:10.5539/mas.v8n3p10 URL: http://dx.doi.org/10.5539/mas.v8n3p10

Abstract

In this paper, the high dielectric constants for Ta_2O_5 (~18.8) and Nb_2O_5 (~25.5) were deposited by a RF reactive magnetron sputtering and respectively annealed at 700 °C and 400 °C O_2 ambiance for 30 min in a conventional furnace. The purpose of this study is to optimize the annealing condition (various temperatures at N_2 or O_2 ambiance) of the high-dielectric-constant Ta_2O_5 and Nb_2O_5 films deposited by RF reactive magnetron sputtering to enhance the dielectric constant of those films to further lower the operating voltage. Based on the results, an electrowetting optical deflector (EOD) filled with the water (1% sodium dodecyl sulfate (SDS)) and dodecane was fabricated and tested, and the contact angle of the inclined liquid surface on the left and right sidewall can be varied about 70° at 9 V operating voltage. This study provides a practical way to fabricate a high dielectric constant layer for low voltage electrowetting on dielectric (EWOD) application.

Keywords: electrowetting optical deflector, anneal, dielectric constant

1. Introduction

Electrowetting phenomenon was first exploited by Lippmann (1875). By varying the voltage between the electrolyte droplet and the substrate, the contact angle of droplet can be modulated. Due to the electrolysis effect, the room to manipulate the contact angle of droplet is very limited. Till Berge (1993) inserted a thin insulating layer between the electrolyte droplet and the electrode to eliminate the electrolysis problem, the contact angle change can be dramatically increased at a large voltage. This improved technology was so called EWOD. Since then, it initiated an explosive growth in electrowetting research, especially in the field of optics (Mugele & Baret, 2005; Kuiper, Hendriks, Hayes, Feenstra, & Baken, 2005; Hou, Zhang, Smith, Yang, & Heikenfeld, 2010; Ceyssensa et al., 2013).

Many studies have used SiO_2 with a low dielectric-constant of about 3.8 as the insulating layer, leading to a large operating voltage of several tens of volts (Smith, Abeysinghe, Haus, & Heikenfeld, 2006; Papathanasiou, Papaioannou, & Boudouvis, 2008; Cho, Fan, Moon, & Kim, 2002; Cho, Moon, & Kim, 2003). The larger operating voltage will cause electrical breakdown and reliability. Thus, in the electrowetting optics application, the low operating voltage is the future trend in order to be compatible with commercial electronic components, reliability and conserve power. Known from Lippmann-Young equation (Mugele & Baret, 2005), decreasing the thickness of the dielectric layer, employing a high dielectric constant material, and minimizing the interfacial surface tension between the electrolyte and the surrounding ambient phase are the three applicable approaches to drop the required operating voltage. However, thinning the dielectric layer tends to induce dielectric breakdown (Berry, Kedzierski, & Abedian, 2006) at high electric field; besides, adding surfactants to the oil-water interface has been proven to slow down the oil-water response time (Roques-Carmes, Palmier, Hayes, & Schlangen, 2005). Therefore, using high dielectric films is the most potential method among the three to achieve the low operating voltage without suffering from other side effects.

A lot of efforts have been dedicated to exploring the deposition of high dielectric constant materials, and promising progress has been reported (Moon, Cho, Garrrell, & Kim, 2002; Li et al., 2008; Chang, Choi, Han, & Pak, 2009; Raj, Dhindsa, Smith, Laughlin, & Heikenfeld, 2009; Lin, Evans, Welch, Hsu, Madison, & Fair, 2010). However, the facilities used in those studies, such as metal-organic chemical vapor deposition (MOCVD) (Moon et al., 2002) and atomic layer deposition (ALD) (Chang, Choi, Han, & Pak, 2009; Raj, Dhindsa, Smith, Laughlin, & Heikenfeld, 2009), are not widely available. As a consequence, some other cost-saving approaches have been suggested for the material deposition. In the dense wavelength division multiplexing (DWDM) system, it required a high dielectric films (e.g., Ta_2O_5, Nb_2O_5, or TiO_2) to fabricate an interference filter. In general, the most common way to deposit these high dielectric layers is by RF reactive magnetron sputtering, and most of the metal oxides can be deposited by using the metal targets and reaction gas mixtures (e.g., O_2 and Ar).

The purpose of this research was to fabricate a high dielectric constant layer to lower the operating voltage. According to Park's findings (Park, Li, Nam, & Rhee, 1999), a high dielectric constant film can be produced by using sputtering and annealing technologies. The purpose of this study is to optimize the annealing condition of the high-dielectric-constant Ta_2O_5 and Nb_2O_5 films deposited by RF reactive magnetron sputtering (Lin et al., 2011; Zhou, Luo, Li, & Liu, 2009; Coskun & Demirel, 2013; Lai, Lin, Huang, Gai, & Qu, 2006) to enhance the dielectric constant of those films to further lower the operating voltage. The annealing was taken at various temperatures under N_2 or O_2 ambiance in a conventional furnace. The dielectric constant of the resulting films was deduced from capacitance measurement with an inductance capacitance resistance (LCR) meter, and the film surface morphologies were investigated with scanning electron microscope (SEM) and atomic force microscope (AFM). Finally, an electrowetting optical deflector (EOD) device (Chen & Fu, 2011) consisting of a 200-nm Nb_2O_5, layer annealed at 400 °C for 30 min under O_2 ambient was fabricated and tested. The contact angle of the inclined liquid with respective to the EOD sidewalls can be varied up to 70° at the operating voltage of 9 V.

2. Experimental Procedures

The cleaning procedures of the substrate for dielectric film deposition were briefed as follows. First, the p-type (100) silicon wafers were immersed in the piranha solutions for 5 min to remove organic contamination, and then dipped in the buffered oxide etch (BOE) for 30 sec to strip off the native oxide. Next, the wafers were rinsed with deionized (DI) water with resistivity of ~18 MΩ, were dehydrated on a hotplate at 200 °C for at least 20 min, and were cooled to room temperature.

The deposition of dielectric films was carried out in a RF magnetron sputtering system, and the tantalum and niobium targets of 99.99% purity were employed for the Ta_2O_5 and Nb_2O_5 film deposition. To start the sputtering process, the system was first evacuated to a base pressure of 0.67 mPa, followed by the Ar and O_2 gases flow with the rates keeping at 27 sccm and 3 sccm, respectively, corresponding to a total gas pressure of 0.4 Pa. Then, the sputtering power was set to be 300 W, and the substrate temperature was raised to 100 °C. The deposition rates for Ta_2O_5 and Nb_2O_5 were 10 and 2 nm/min, respectively. The dielectric layers with thicknesses of 200 nm were prepared for each material, and the thickness of each coated layer was measured with a surface profile meter (AMBIOS XP-1). Finally, these samples were respectively annealed in a conventional N_2 or O_2 furnace using at temperatures ranging from 400 °C to 1000 °C for 30 min. After annealing procedure, the samples were cooled down to room temperature.

The dielectric constant, surface morphologies, and surface roughness for the resulting dielectric films were respectively analyzed by the LCR (Agilent E4980A) meter, SEM (Hitachi S-4800), and AFM (Veeco) before and after annealing. In order to measure dielectric constants, a metal-insulator-semiconductor (MIS) capacitor with a 500 × 500 μm^2 Al pad was fabricated on top of the dielectric layer using photolithography and lift-off process. The p-type Si substrate was positive biased, and the Al pad was negative biased. The dielectric constant of the resulting films was deduced from capacitance measurement at various frequencies (100 Hz ~100 kHz) and bias (50 mV, 250 mV, and 1 V) with the LCR meter. To calculate the dielectric constant, the post-annealing sample thickness was measured by its cross-sectional SEM image. The surface roughness of dielectric films was analyzed by tapping mode AFM, and the scan area was 1 × 1 μm^2.

An EOD device was fabricated to test the contact angle change of the inclined liquid surface on the sidewalls. The detail fabrication processes have been reported elsewhere (Kuiper et al., 2005; Smith, 2006; Chen et al., 2011). As shown in Figure 1(a), an EOD chamber included two Si sidewalls (coated with a composite dielectric layer) as electrodes, a transparent indium tin oxide (ITO) glass spacer (~3 mm wide) in the bottom, a top glass plate, and two front and back sealing glass plates. The composite dielectric layers was a 200-nm Nb_2O_5 dielectric layer (annealed at 400 °C O_2 ambiance for 30 min) covered by a 100 nm CYTOP® hydrophobic fluoropolymer.

After assembling, the EOD chamber was filled with water (containing 1% SDS) and dodecane, and the liquid-liquid interface formed a convex shape (Figure 1(a)). Figure 1(b) shows the schematic of the voltage connections and liquid incline angle measurement system. The experimental flow chart is shown in Figure 2. The EOD's operation required three electrical terminals: two DC voltage sources (V_L and V_R) attached to the Si electrodes, and the bottom ITO electrode was electrically grounded. The EOD device was operated in one of the three modes: $V_L = V_R$, $V_L > V_R$, and $V_L < V_R$. The contact angles of the inclined liquid surface on the left and right sidewalls were indicated by θ_L and θ_R, and were measured by a charge coupled device (CCD) image capturing system.

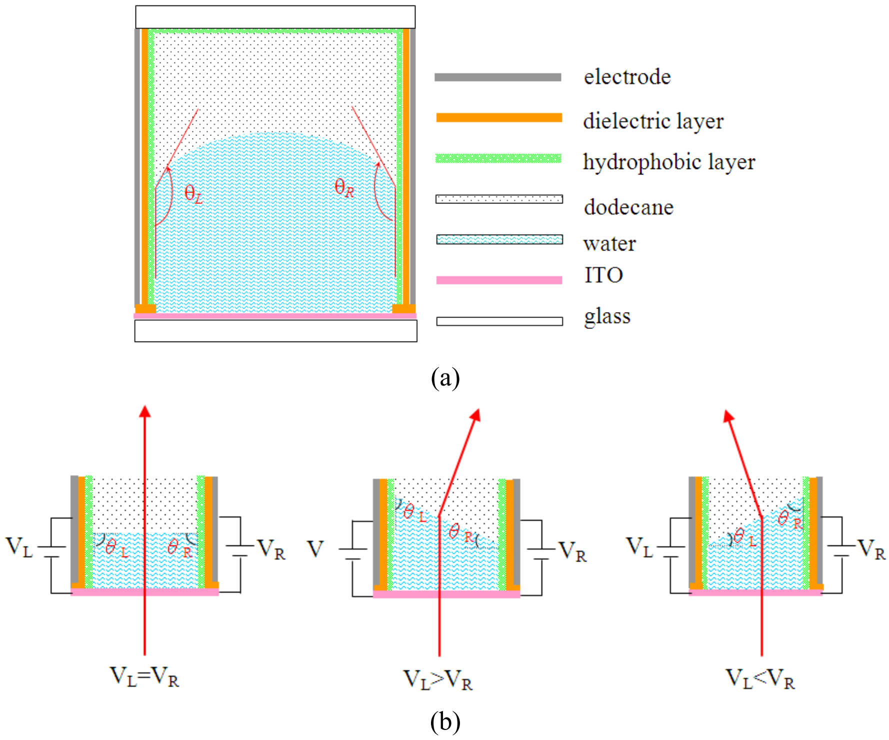

Figure 1. The schematic of (a) a basic EOD device structure; and (b) the three operating modes of an EOD device: V_L=V_R, V_L>V_R, and V_L<V_R from left to right

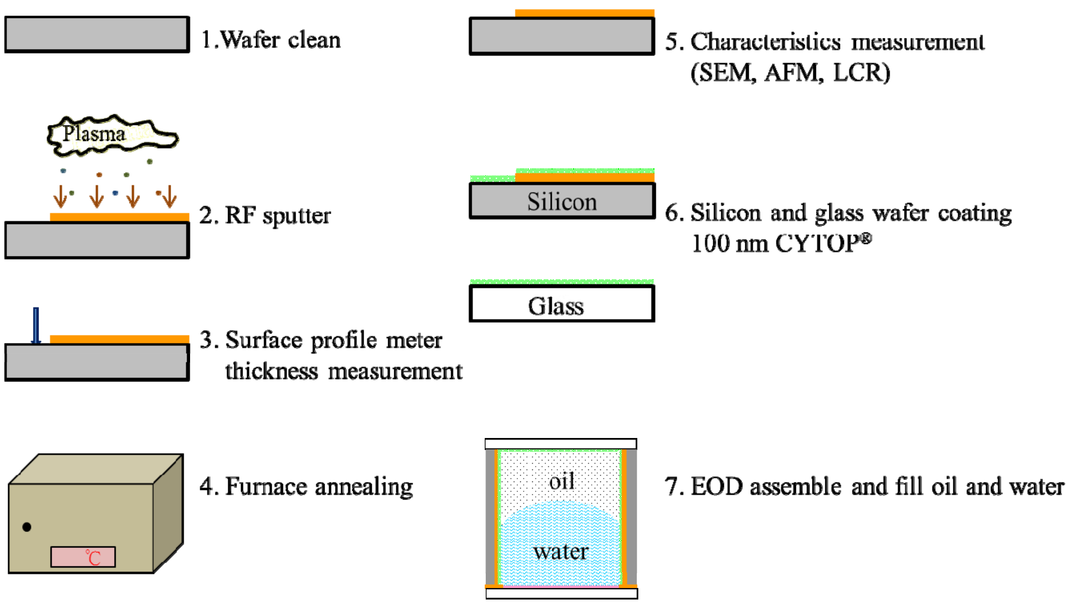

Figure 2. The experimental flow chart

3. Results and Discussion

3.1 Dielectric Constant Characteristics

The thin film deposited by RF reactive magnetron sputtering will form amorphous atoms or ions randomly, and there are dangling bonds and voids. When annealing to certain temperature, the thin film will crystalline and improve crystal imperfections (defect, impurity) to enhance the dielectric constant. To Achieve such a new material could benefit all EWOD devices in terms of lower voltage, east to fabricate and improved reliability.

Figures 3 and 4 illustrate the dielectric constant as a function of various N_2 and O_2 ambient annealing temperatures for Ta_2O_5 and Nb_2O_5. The measuring frequency was fixed at 100 Hz, and measuring voltages were varied from 50 mV to 1 V. The results show that the dielectric constant was found to slightly vary as the measuring voltage increased. This was due to the reason that the MIS capacitance was biased at the accumulation mode voltages.

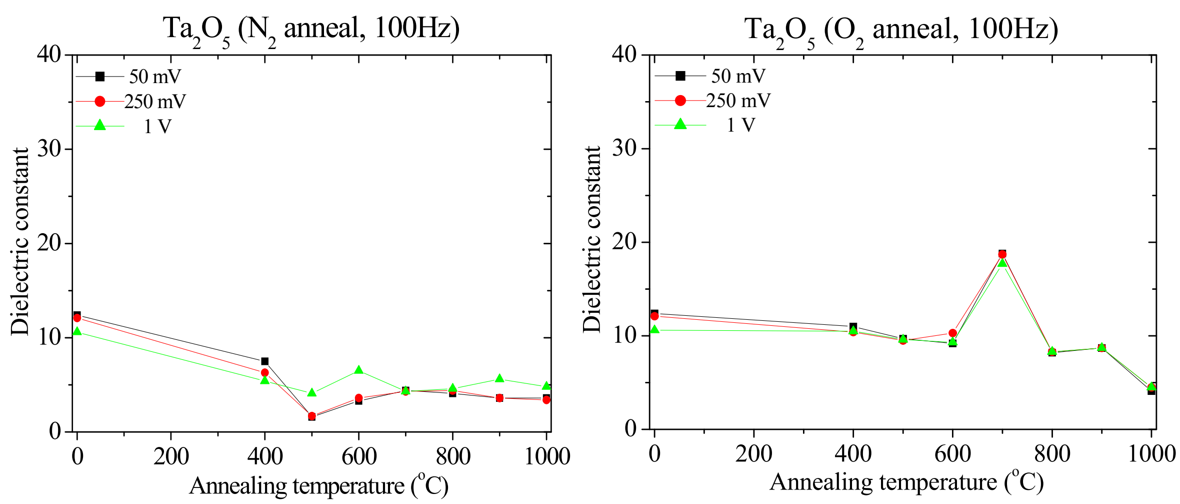

(a) (b)

Figure 3. Ta_2O_5 dielectric constant as a function of (a) N_2; and (b) O_2 annealing temperatures. The measuring frequency was fixed at 100 Hz, and measuring voltages were varied from 50 mV to 1 V. The zero annealing temperature indicates the as-deposited samples

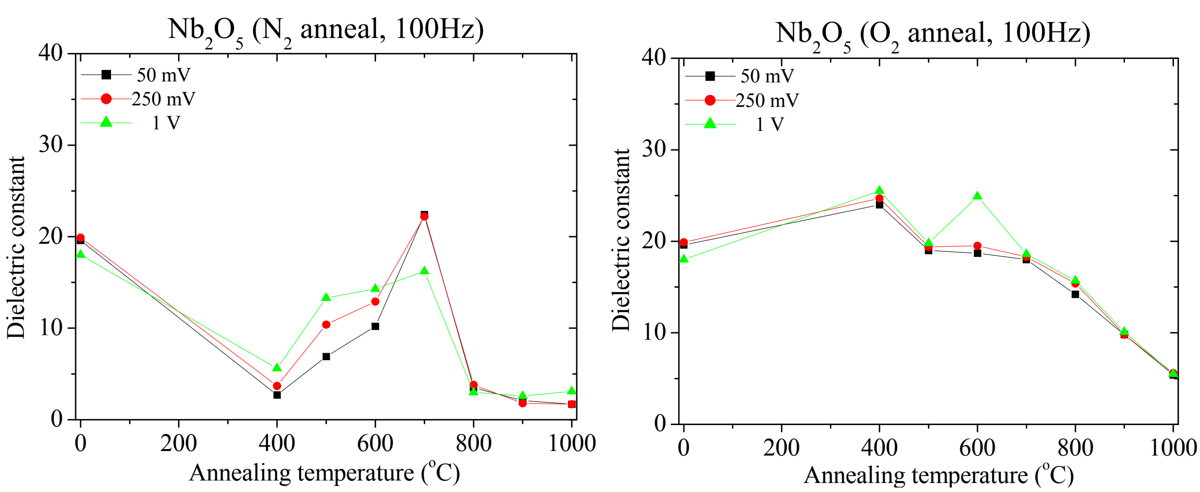

(a) (b)

Figure 4. Nb_2O_5 dielectric constant as a function of (a) N_2; and (b) O_2 annealing temperatures. The measuring frequency was fixed at 100 Hz, and measuring voltages were varied from 50 mV to 1 V. The zero annealing temperature indicates the as-deposited samples

Figures 5 and 6 illustrate the dielectric constant as a function of various measuring frequencies (100 Hz ~ 100 kHz) and annealing temperatures (400 °C ~ 1000 °C) for Ta_2O_5 and Nb_2O_5. The measuring voltage was fixed at 1 V, and the dielectric constant was found to decrease as the measuring frequency increased (Joshi & Cole, 1999). Moreover, Figures 5(a) and 6(a) show that annealed in the N_2 temperature did not enhance much the dielectric constants than as-deposited dielectric films, and Figures 5(b) and 6(b) show that annealed in the O_2 temperature can enhance the dielectric constants at certain temperature.

From the Figure 5(b) and 6(b) we selected the best conditioning for Ta_2O_5 (~18.8 at 700 °C) and Nb_2O_5 (~ 25.5 at 400 °C) with O_2 annealing. Figure 7 shows the dielectric constants of the optimized films when the measuring frequencies were varied from 100 Hz to 100 kHz, and measuring voltages were varied from 50 mV to 1 V. The results indicate that the dielectric constant decreased as the measuring frequency increased. These findings were in good agreement with those reported (Joshi et al., 1999; Masse, Szymanowski, Zabeida, Amassian, Klemberg-Sapieha, & Martinu, 2006) for Ta_2O_5 and Nb_2O_5. The literature (Shinriki, Nishioka, Ohji, & Mukai, 1989) shows that Ta_2O_5 and Nb_2O_5 films crystallize at 650 °C and 450 °C to form a hexagonal structure and enhance the dielectric constant.

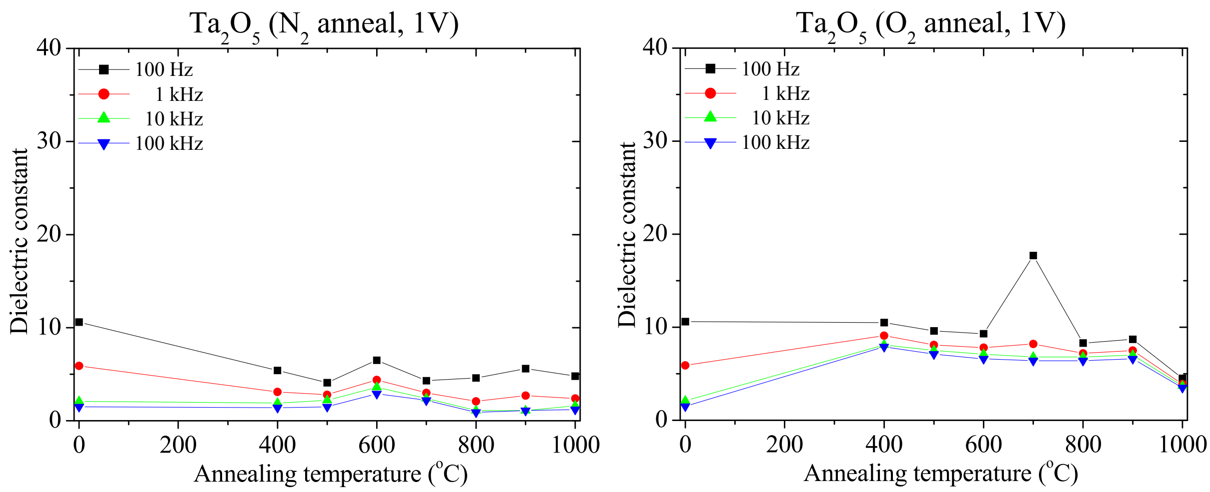

(a) (b)

Figure 5. Ta_2O_5 dielectric constant as a function of (a) N_2; and (b) O_2 annealing temperatures. The measuring voltage was fixed at 1 V, and measuring frequencies were varied from 100 Hz to 100 kHz. The zero annealing temperature indicates the as-deposited samples

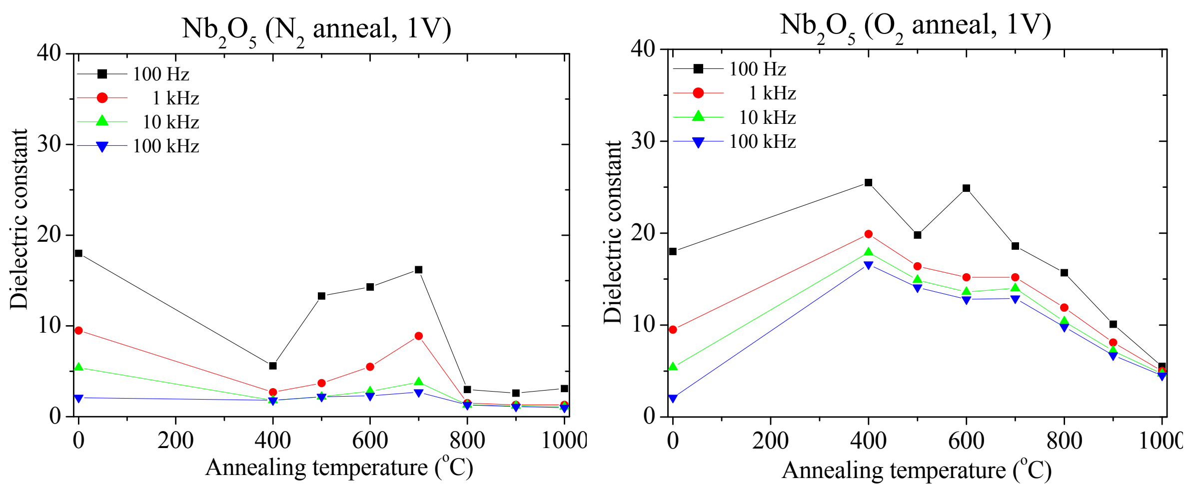

(a) (b)

Figure 6. Nb_2O_5 dielectric constant as a function of (a) N_2; and (b) O_2 annealing temperatures. The measuring voltage was fixed at 1 V, and measuring frequencies were varied from 100 Hz to 100 kHz. The zero annealing temperature indicates the as-deposited samples

Besides, in these oxidation processes (annealing temperature ≧900 °C), the dielectric constant was reduced due to the growth of a SiO_2 film, which has a small dielectric constant (3.8), between the dielectric film and the silicon substrate. This can explain the reason that dielectric constant decreased as the annealing temperature increased.

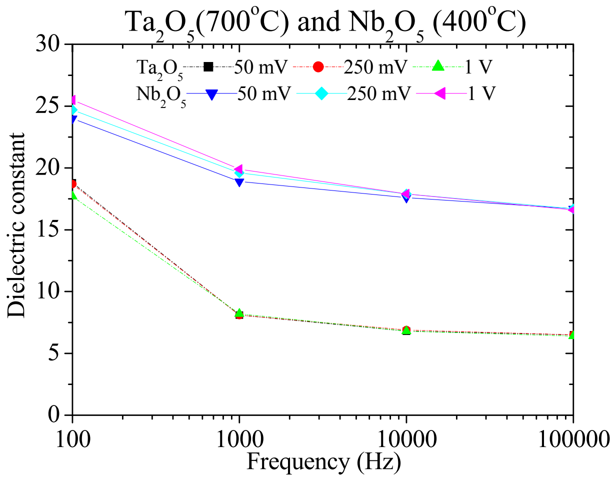

Figure 7. The dielectric constant as a function of measuring frequencies with O_2 annealing temperature at (a) 700 °C Ta_2O_5; and (b) 700 °C Nb_2O_5. The measuring voltages were varied from 50 mV to 1 V

3.2 Surface Morphology Features

Figures 8-11 show the SEM and AFM images of the dielectric film for as deposited and annealed at various temperatures. As shown in Figures 8(a) and 10(a), the surface morphology of the Ta_2O_5 and Nb_2O_5 films was smooth and no defects. Figure 12 displays the average roughness values as a function of N_2 and O_2 annealing temperatures for Ta_2O_5 and Nb_2O_5 dielectric films. The results show that the surface roughness rose as the annealing temperature increased. The surface roughness change for Ta_2O_5 (0.42 nm ~ 1.93 nm) was much smaller than the Nb_2O_5 (0.51 nm ~ 9.06 nm) under various N_2 and O_2 annealing temperatures.

The surface roughness for as deposited Ta_2O_5 and Nb_2O_5 dielectric films was very small (≦0.51 nm); however, when the annealing temperature was gradually increased, the surface of the dielectric layers began to form grain boundary (see Figures 8(b) and 10(b)) and the surface roughness was increased. In the Ta_2O_5 dielectric film, the grain boundary did not form much as the anneal temperatures were below 650 °C; while, when the annealing temperature was above 450 °C, the Nb_2O_5 dielectric film formed a distinct grain boundary (Masse et al., 2006). The surface roughness for the highest dielectric constant conditions of Ta_2O_5 (at 700 °C O_2 annealing) and Nb_2O_5 (at 400 °C O_2 annealing) was 0.65 nm and 1.15 nm, respectively. The surface roughness affects the contact angle and contact angle hysteresis (the difference between forward and backward contact angle). In our case, the low surface roughness is needed to avoid reliability problems.

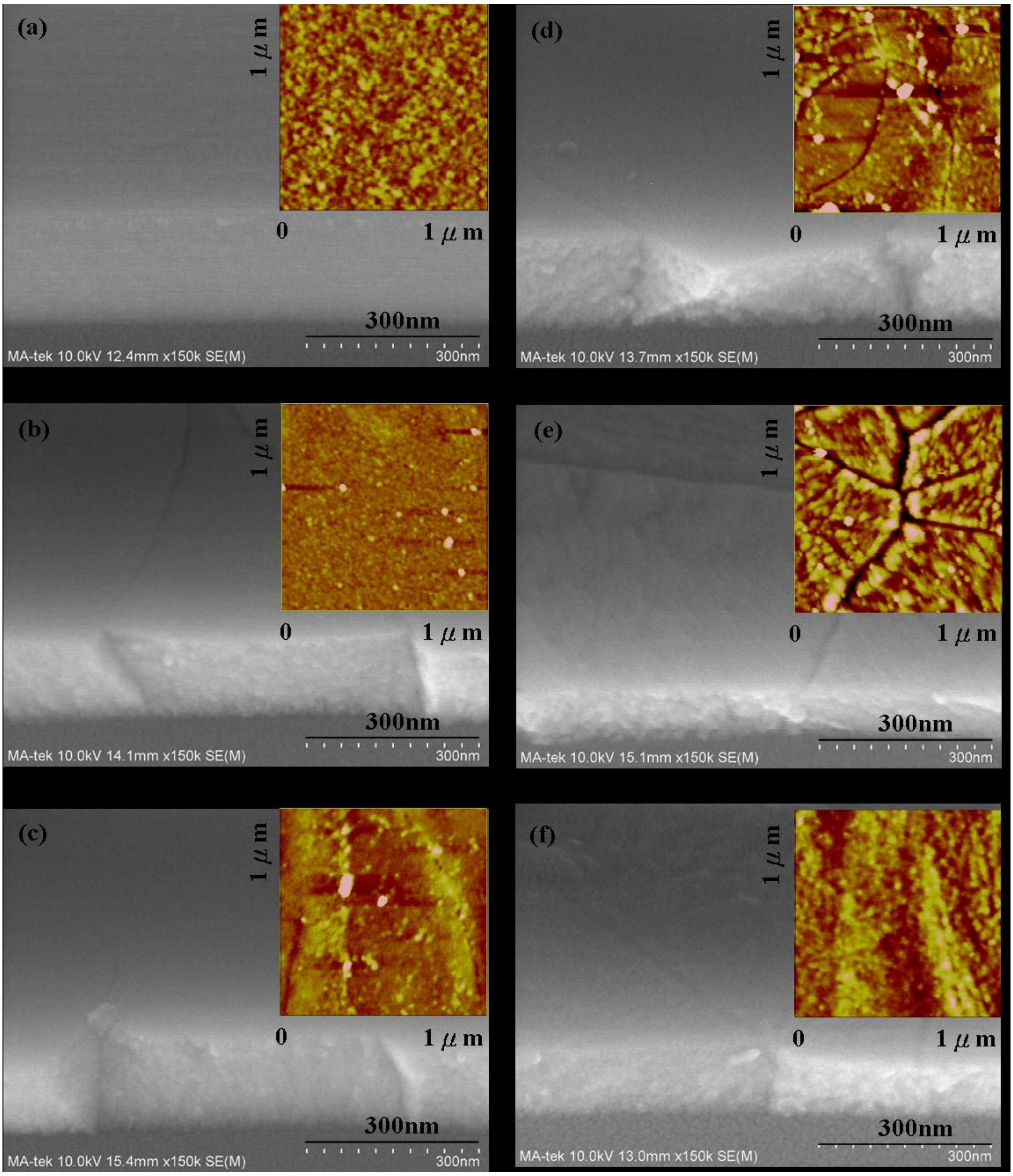

Figure 8. The SEM images show the surface morphology of the Ta_2O_5 film for (a) as deposited, and with N_2 annealing at (b) 400 °C; (c) 600 °C (d) 700 °C; (e) 800 °C; and (f) 1000 °C. The inset picture is the AFM image with 1μm × 1μm area

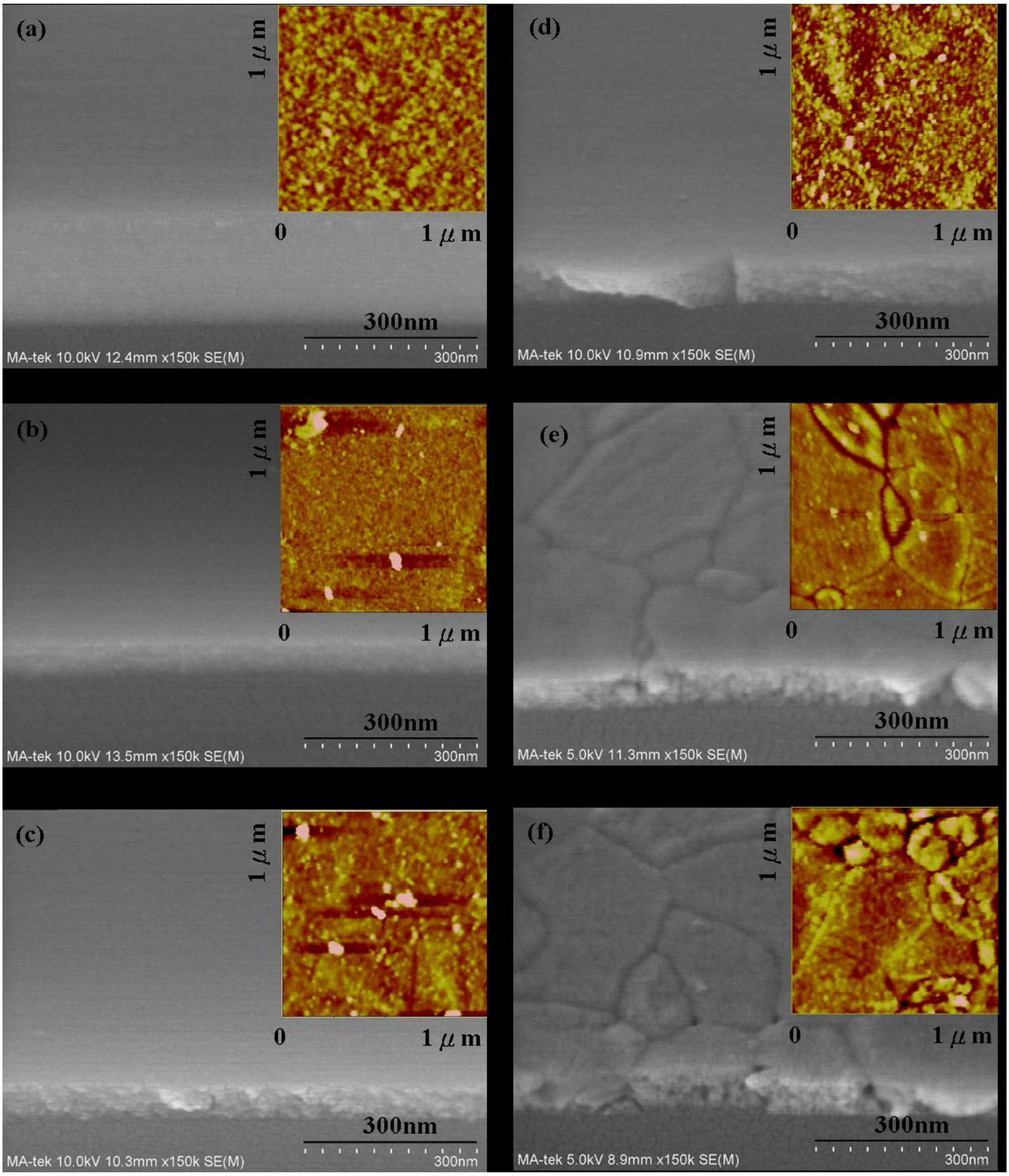

Figure 9. The SEM images show the surface morphology of the Ta_2O_5 film for (a) as deposited, and with O_2 annealing at (b) 400 °C; (c) 600 °C (d) 700 °C; (e) 800 °C; and (f) 1000 °C. The inset picture is the AFM image with 1μm × 1μm area

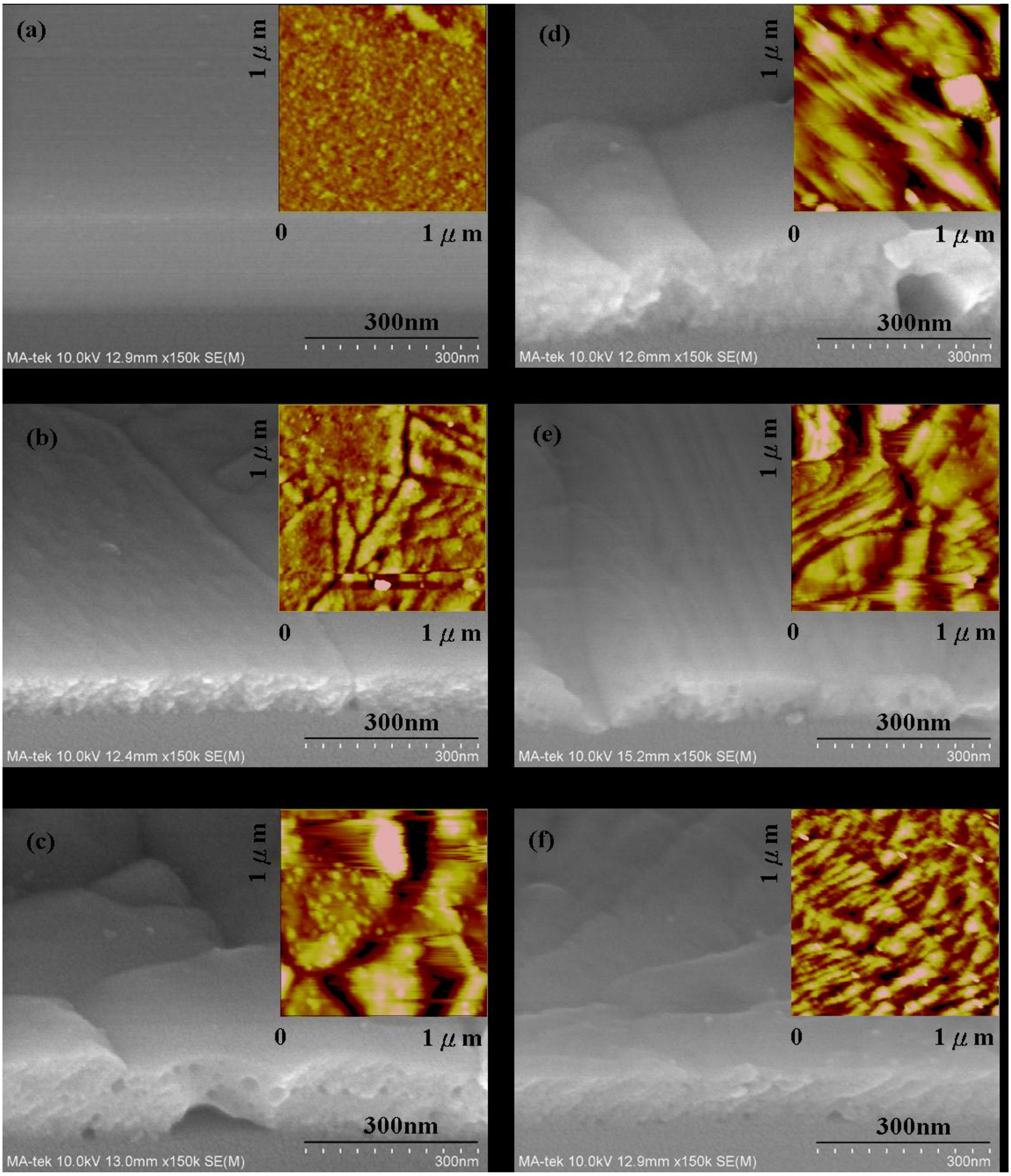

Figure 10. The SEM images show the surface morphology of the Nb_2O_5 film for (a) as deposited, and with N_2 annealing at (b) 400 °C; (c) 600 °C (d) 700 °C; (e) 800 °C; and (f) 1000 °C. The inset picture is the AFM image with 1μm × 1μm area

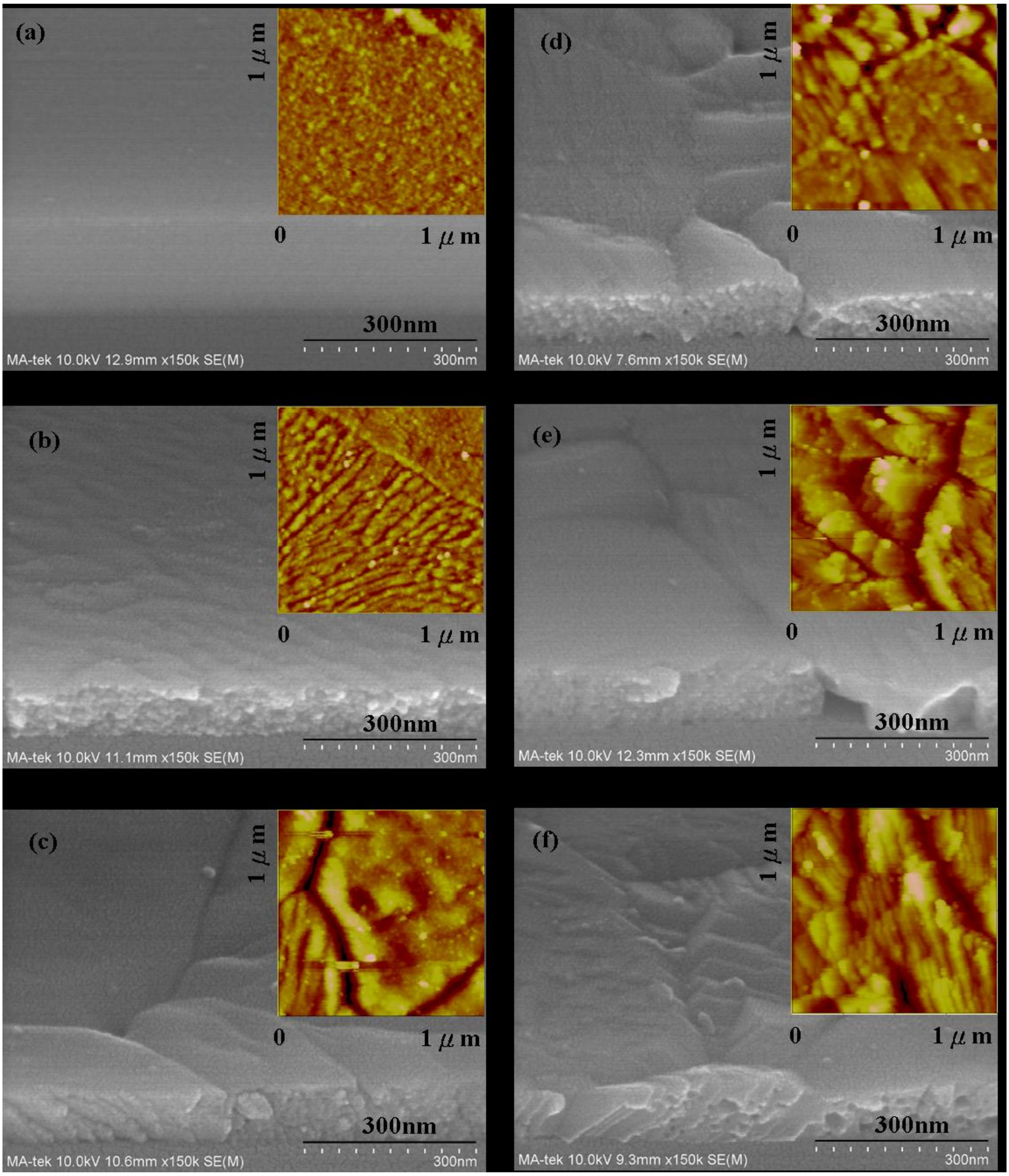

Figure 11. The SEM images show the surface morphology of the Nb_2O_5 film for (a) as deposited, and with O_2 annealing at (b) 400 °C; (c) 600 °C (d) 700 °C; (e) 800 °C; and (f) 1000 °C. The inset picture is the AFM image with 1μm × 1μm area

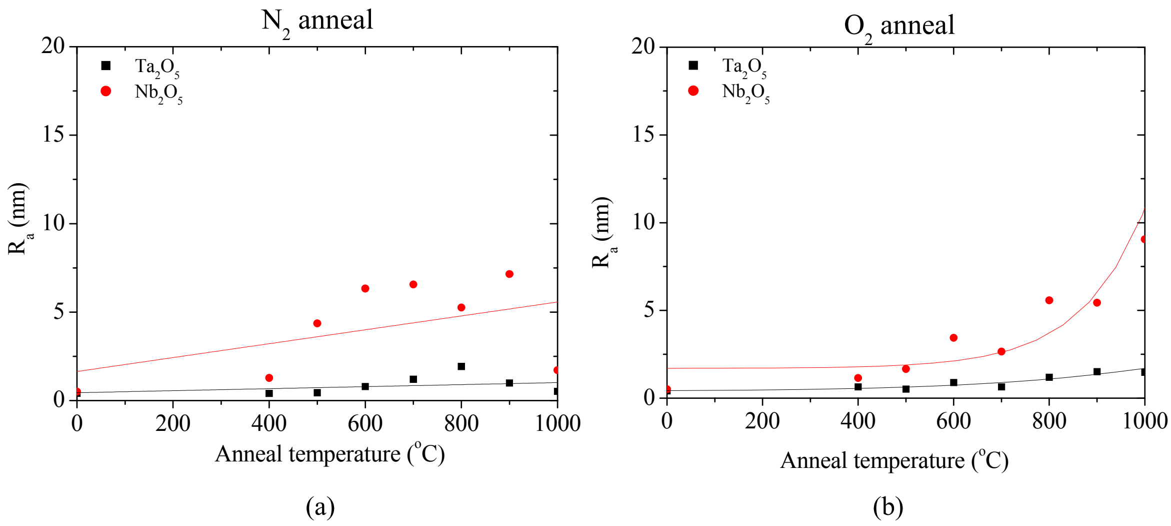

Figure 12. Average roughness as a function of (a) N_2; and (b) O_2 annealed temperatures for Ta_2O_5 and Nb_2O_5 dielectric films (by AFM measurement)

3.3 Demonstration of EOD Deflection

Figure 13 shows the photographs of the EOD device in various operating voltages. When the EOD device was filled inside with the water (1% SDS) and dodecane at zero voltage, the liquid-liquid interface formed a convex shaped meniscus (Figure 13(a)). When the left and right sidewalls biased at 7 V, the liquid-liquid interface become level (Figure 13(b)). In addition, when the V_L = 9 V and V_R = 5 V, the liquid-liquid interface inclined to the upper left corner (Figure 13(c)). Reversing the bias voltage, the liquid-liquid interface inverted to the upper right corner (Figure 13(d)) (Video, 4.11 MB).

Experimental results show that the contact angle of the inclined liquid surface on the two EOD sidewalls can vary about 70° at 9 V operating in a dodecane/water/Cytop®/Nb_2O_5 system, and which was reduced 2 V operating voltage compared to our previous study (Ta_2O_5 without annealing treatment) (Chen et al., 2011).

Due to the contact angle saturation phenomenon, the contact angle of the inclined liquid surface was saturated at 70°. In future work, applying an AC operating voltage (Nanayakkara et al., 2010) and a high quality dielectric film (pinhole free) to avoid charges trapping (Verheijen & Prins, 1999) will reduce contact angle saturation. This paper may provide a good reference for the dielectric constant characteristics in the AC operating voltage.

4. Conclusions

The high dielectric constant layers (Ta_2O_5 and Nb_2O_5) were deposited on the silicon substrate by a RF reactive magnetron sputtering and annealed at various temperatures under N_2 or O_2 ambiance in a conventional furnace. The dielectric constant and surface roughness of the dielectric layers before and after various annealing treatments were studied by an LCR meter, SEM and AFM instruments. The as-deposited dielectric films have an amorphous structure, and the surface roughness is very small (≦0.51 nm). However, when the annealing temperature was gradually increased, the surface of the dielectric layers began to form grain boundary and the surface roughness becomes larger. Experimental results show that annealed in the N_2 ambiance did not enhance the dielectric constant than as-deposited dielectric films, but annealed in the O_2 ambiance can enhance the dielectric constants below certain temperature.

This study gets the high dielectric constants for Ta_2O_5 (~18.8) and Nb_2O_5 (~25.5) deposited by a RF reactive magnetron sputtering and respectively annealed at 700 °C and 400 °C O_2 ambiance for 30 min in a conventional furnace. Moreover, we show that the contact angle of EOD device can change 70° for a dodecane/water/Cytop®/Nb_2O_5/Si system with an applied voltage as low as 9 V.

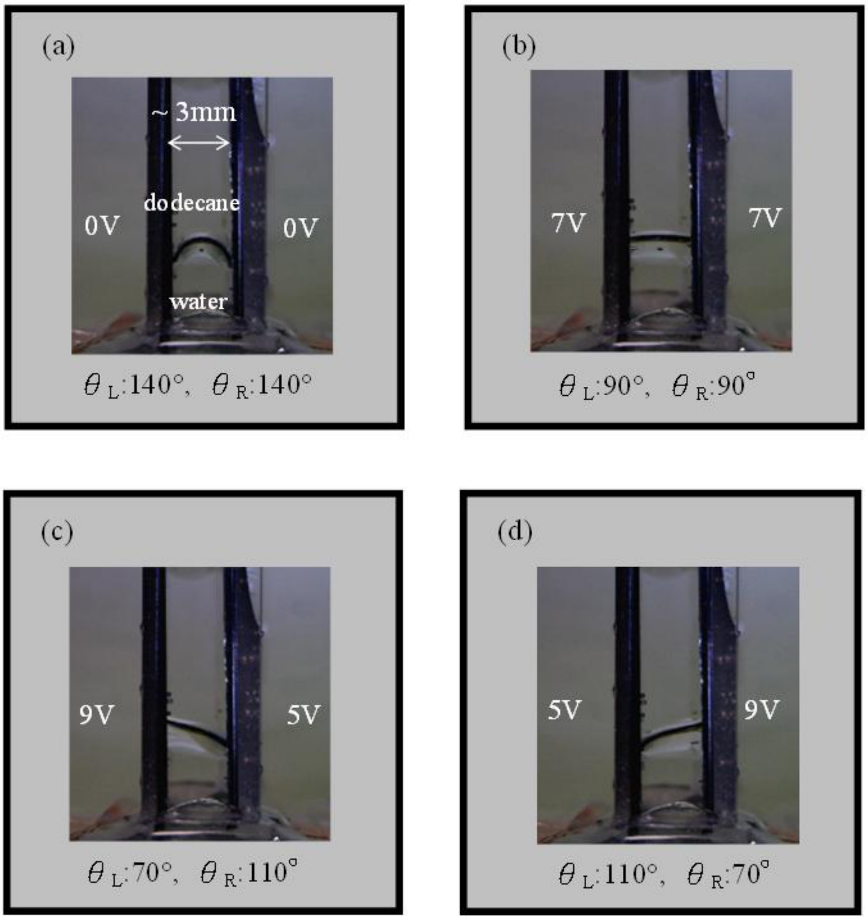

Figure 13. Side view photographs of the EOD device (dodecane and 1%SDS water) with (a) $V_L = V_R = 0$ V; (b) $V_L = V_R = 7$ V; (c) $V_L = 9$ V, $V_R = 5$ V; and (d) $V_L = 5$ V, $V_R = 9$ V. The water is electrically grounded (Video, 4.11 MB)

Acknowledgements

The authors gratefully acknowledge their colleagues Dr. Chiun-Lung Tsai for valuable discussions and comments on the manuscript. Specials thanks are due to Ms. Ming-Fang Hsu for AFM measurement. The research is financially supported mainly by ITRI (Industrial Technology Research Institute, Taiwan).

References

Berge, B. (1993). Electrocapillarity and wetting of insulator films by water. *Comptes Rendus De L Academie Des Sciences Serie II, 317*(2), 157-163.

Berry, S., Kedzierski, J., & Abedian, B. (2006). Low voltage electrowetting using thin fluoroploymer films. *Journal of Colloid and Interface Science, 303*(2), 517-524. http://dx.doi.org/10.1016/j.jcis.2006.08.004

Ceyssens, F., Witters, D., Van Grimbergen, T., Knez, K., Lammertyn, J., & Puers, R. (2013). Integrating optical waveguides in electrowetting-on-dielectric digital microfluidic chips. *Sensors and Actuators B: Chemical, 181*, 166-171. http://dx.doi.org/10.1016/j.snb.2013.01.078

Chang, J. H., Choi, D. Y., Han, S., & Pak, J. J. (2010). Driving characteristics of the electrowetting-on-dielectric device using atomic-layer-deposited aluminum oxide as the dielectric. *Microfluidics and Nanofluidics, 8*(2), 269-273. http://dx.doi.org/10.1007/s10404-009-0511-9

Chen, H. H., & Fu, C. C. (2011). Low Voltage Electrowetting Optical Deflector. *Japanese Journal of Applied Physics, 50*(2011) 037202. http://dx.doi.org/10.1143/JJAP.50.037202

Cho, S. K., Fan, S. K., Moon, H., & Kim, C. J. (2002, January). Towards digital microfluidic circuits: creating, transporting, cutting and merging liquid droplets by electrowetting-based actuation. In *Micro Electro Mechanical Systems, 2002. The Fifteenth IEEE International Conference on* (pp. 32-35). IEEE.

Cho, S. K., Moon, H., & Kim, C. J. (2003). Creating, transporting, cutting, and merging liquid droplets by electrowetting-based actuation for digital microfluidic circuits. *Microelectromechanical Systems, Journal of, 12*(1), 70-80. http://dx.doi.org/10.1109/JMEMS.2002.807467

Coşkun, Ö. D., & Demirela, S. (2013). The optical and structural properties of amorphous Nb2O5 thin filmsprepared by RF magnetron sputtering. *Applied Surface Science, 277*, 35-39. http://dx.doi.org/10.1016/j.apsusc.2013.03.116

Hou, L., Zhang, J., Smith, N., Yang, J., & Heikenfeld, J. (2010). A full description of a scalable microfabrication process for arrayed electrowetting microprisms. *Journal of Micromechanics and Microengineering, 20*(1), 015044. http://dx.doi.org/10.1088/0960-1317/20/1/015044

Joshi, P. C., & Cole, M. W. (1999). Influence of postdeposition annealing on the enhanced structural and electrical properties of amorphous and crystalline Ta_2O_5 thin films for dynamic random access memory applications. *Journal of Applied Physics, 86*(2), 871-880. http://dx.doi.org/10.1063/1.370817

Kuiper, S., Hendriks, B. H. W., Hayes, R. A., Feenstra, B. J., & Baken, J. M. E. (2005, August). Electrowetting-based optics. In *Optics & Photonics 2005* (pp. 59080R-59080R). International Society for Optics and Photonics.

Lai, F., Lin, L., Huang, Z., Gai, R., & Qu, Y. (2006). Effect of thickness on the structure, morphology and optical properties of sputter deposited Nb2O5 films. *Applied Surface Science, 253*(4), 1801-1805. http://dx.doi.org/10.1016/j.apsusc.2006.03.014

Li, Y., Parkes, W., Haworth, L. I., Stokes, A. A., Muir, K. R., Li, P., … Walton, A. J. (2008). Anodic Ta2O5 for CMOS compatible low voltage electrowetting-on-dielectric device fabrication. *Solid State Electronic, 52*(9), 1382-1387. http://dx.doi.org/10.1016/j.sse.2008.04.030

Lin, Y. Y., Evans, R. D., Welch, E., Hsu, B. N., Madison, A. C., & Fair, R. B. (2010). Low voltage electrowetting-on-dielectric platform using multi-layer insulators. *Sensors and Actuators B: Chemical, 150*(1), 465-470. http://dx.doi.org/10.1016/j.snb.2010.06.059

Lin, Y. Y., Evans, R. D., Welch, E., Hsu, B. N., Madison, A. C., & Fair, R. B. (2011). Low Voltage Electrowetting-on-Dielectric Platform using Multi-Layer Insulators. Sens Actuators B Chem. Author manuscript; available in PMC Sep 21, 2011.

Lippmann, G. (1875). *Relations entre les phénomènes électriques et capillaires. Ann. Chim. Phys., 5*, 494.

Masse, J. P., Szymanowski, H., Zabeida, O., Amassian, A., Klemberg-Sapieha, J. E., & Martinu, L. (2006). Stability and effect of annealing on the optical properties of plasma-deposited Ta_2O_5 and Nb_2O_5 films. *Thin Solid Films, 515*(4), 1674-1682. http://dx.doi.org/10.1016/j.tsf.2006.05.047

Moon, H., Cho, S. K., & Garrell, R. L. (2002). Low voltage electrowetting-on-dielectric. *Journal of Applied Physics, 92*(7), 4080-4087. http://dx.doi.org/10.1063/1.1504171

Mugele, F., & Baret, J. C. (2005). Electrowetting: from basics to applications. *Journal of Physics: Condensed Matter, 17*(28), R705. http://dx.doi.org/10.1088/0953-8984/17/28/R01

Nanayakkara, Y. S., Perera, S., Bindiganavale, S., Wanigasekara, E., Moon, H., & Armstrong, D. W. (2010). The effect of AC frequency on the electrowetting behavior of ionic liquids. *Analytical Chemistry, 82*(8), 3146-3154. http://dx.doi.org/10.1021/ac9021852

Papathanasiou, A. G., Papaioannou, A. T., & Boudouvis, A. G. (2008). Illuminating the connection between contact angle saturation and dielectric breakdown in electrowetting through leakage current measurementsa). *Journal of Applied Physics, 103*(3), 034901. http://dx.doi.org/10.1063/1.2837100

Park, Y. B., Li, X., Nam, G. J., & Rhee, S. W. (1999). Effects of annealing in O_2 and N_2 on the microstructure of metal organic chemical vapor deposition Ta_2O_5 film and the interfacial SiO_2 layer. *Journal of Materials Science: Materials in Electronics, 10*(2), 113-119. http://dx.doi.org/10.1023/A:1008960014883

Raj, B., Dhindsa, M., Smith, N. R., Laughlin, R., & Heikenfeld, J. (2009). Ion and liquid dependent dielectric failure in electrowetting systems. *Langmuir, 25*(20), 12387-12392. http://dx.doi.org/10.1021/la9016933

Roques-Carmes, T., Palmier, S., Hayes, R. A., & Schlangen, L. J. (2005). The effect of the oil/water interfacial tension on electrowetting driven fluid motion. *Colloids and Surfaces A: Physicochemical and Engineering Aspects, 267*(1), 56-63. http://dx.doi.org/10.1016/j.colsurfa.2005.06.056

Shinriki, H., Nishioka, Y., Ohji, Y., & Mukai, K. (1989). Oxidized Ta_2O_5/Si_3N_4 dielectric films on poly-crystalline Si for dRAMs. *Electron Devices, IEEE Transactions on, 36*(2), 328-332. http://dx.doi.org/10.1109/16.19933

Smith, N. R., Abeysinghe, D. C., Haus, J. W., & Heikenfeld, J. (2006). Agile wide-angle beam steering with electrowetting microprisms. *Optics Express, 14*(14), 6557-6563. http://dx.doi.org/10.1364/OE.14.006557

Verheijen, H. J. J., & Prins, M. W. J. (1999). Reversible electrowetting and trapping of charge: model and experiments. *Langmuir, 15*(20), 6616-6620. http://dx.doi.org/10.1021/la990548n

Zhou, J. C., Luo, D. T., Li, Y. Z., & Liu, Z. (2009). Effect of sputtering pressure and rapid thermal annealing on optical properties of Ta_2O_5 thin films. *Transactions of Nonferrous Metals Society of China, 19*(2), 359-363. http://dx.doi.org/10.1016/S1003-6326(08)60278-2

Copyrights